The Astrophysical Journal Letters, 901:L38 (8pp), 2020 October 1 https://doi.org/10.3847/2041-8213/abb66f

The Relative Role of Bars and Galaxy Environments in AGN Triggering of SDSS Spirals

Minbae Kim and Yun-Young Choi
School of Space Research, Kyung Hee University, Yongin, Gyeonggi 17104, Republic of Korea; yy.choi@khu.ac.kr
Received 2020 June 5; revised 2020 August 27; accepted 2020 August 28; published 2020 October 1

Abstract

We quantify the relative role of galaxy environment and bar presence on AGN triggering in face-on spiral galaxies using a volume-limited sample with $0.02 < z < 0.055$, $M_r < 19.5$, and $\sigma > 70$ km s^{-1} selected from Sloan Digital Sky Survey (SDSS) Data Release 7. To separate their possible entangled effects, we divide the sample into bar and non-bar samples, and each sample is further divided into three environment cases of isolated galaxies, interacting galaxies with a pair, and cluster galaxies. The isolated case is used as a control sample. For these six cases, we measure AGN fractions at a fixed central star formation rate and central velocity dispersion, σ. We demonstrate that the internal process of the bar-induced gas inflow is more efficient in AGN triggering than the external mechanism of the galaxy interactions in groups and cluster outskirts. The significant effects of bar instability and galaxy environments are found in galaxies with a relatively less massive bulge. We conclude that from the perspective of AGN–galaxy coevolution, a massive black hole is one of the key drivers of spiral galaxy evolution. If it is not met, a bar instability helps the evolution, and in the absence of bars, galaxy interactions/mergers become important. In other words, in the presence of a massive central engine, the role of the two gas inflow mechanisms is reduced or almost disappears. We also find that bars in massive galaxies are very decisive in increasing AGN fractions when the host galaxies are inside clusters.

Unified Astronomy Thesaurus concepts: Galaxy evolution (594); Galaxy nuclei (609); Galaxy quenching (2040); Galaxy interactions (600); Galaxy clusters (584)

1. Introduction

Active galactic nuclei (AGNs) are powered by gas accretion onto a central supermassive black hole (SMBH; Lynden-Bell 1979; Rees 1984). According to the standard paradigm, AGN activity is expected to be closely related to the mechanism of the gas inflow into the nuclear region. Given the formation and evolution of spiral galaxies, possible mechanisms are broadly classified into two categories: (1) external processes such as galaxy interactions, major mergers (Sanders et al. 1988; Springel et al. 2005; Kim et al. 2020a), and minor mergers (Roos 1981; Hernquist & Mihos 1995); (2) internal dynamical processes such as turbulence of the interstellar medium (ISM) in galactic disks (Wada et al. 2009), stellar wind (Ciotti & Ostriker 2007; Davies et al. 2012), and tidal torques due to nonaxisymmetric perturbations such as bars (Friedli & Benz 1993; Athanassoula 2003).

The large volume-limited galaxy sample obtained from the Sloan Digital Sky Survey (SDSS) makes it possible to conduct many statistical studies that compare changes in AGN fractions with different galaxy properties, bar presence, and various galaxy environments. It has been shown that AGN activity is closely related to the gas inflow mechanisms of bar instability (Oh et al. 2012; Alonso et al. 2013; Galloway et al. 2015; Kim et al. 2020b), galaxy interactions/mergers (Ellison et al. 2011; Hwang et al. 2012; Goulding et al. 2018; Kim et al. 2020a), and high-local-density environments (Gilmour et al. 2007; Sivakoff et al. 2008; Pimbblet & Jensen 2012; Sabater et al. 2013).

These investigations are essential for understanding galaxy formation and evolution, but there is still no clear understanding of the observed galaxy–AGN coevolution. Here, we focus on the fact that external processes affect physical quantities (Blanton et al. 2005a; Park & Choi 2009; Park & Hwang 2009; Li et al. 2019) and bar presence (Eskridge et al. 2000; van den Bergh 2002; Lee et al. 2012), and ultimately control the central gas supply to the galactic center (e.g., Sabater et al. 2015). The entanglement between these three primary factors may have provoked conflicting observational results that depend on sample selection.

In this study, we aim to investigate the direct link between AGN and galaxy evolution after minimizing the possible entanglement by dividing the sample into subsamples that can allow as to isolate the effect of each of the three primary factors. To this end, we first divide the sample into two categories—barred and non-barred. Then, each category is subdivided into three subsets based on the environment—isolated, groups, and clusters. Thus, we obtain a total of six subsamples. For each subsample, we measure AGN fractions at a fixed central velocity dispersion and central star formation rate (SFR) and compare the results. Finally, we quantify the relative roles of the gas transport mechanisms.

2. Observational Data and Sample Selection

We select a volume-limited sample with an r-band absolute magnitude $M_r < -19.5$ and redshifts $0.020 < z < 0.055$ selected from the Sloan Digital Sky Survey Data Release 7 (SDSS DR7; Abazajian et al. 2009). The fiber star formation rates, SFR_{fib}, are obtained from the Max Planck Institute for Astrophysics and the Johns Hopkins University (MPA/JHU) DR8 catalog (Brinchmann et al. 2004). The stellar velocity dispersion, σ, is adopted from the New York University Value-Added Galaxy Catalog (Blanton et al. 2005b). A simple aperture correction of σ is made using the formula of Bernardi et al. (2003). Here, we use only galaxies with $\sigma > 70$ km s^{-1} to avoid a selection effect due to the [O III] flux limit in

detecting the AGN. The σ and M_r cuts exclude many disk-dominated and irregular late-type galaxies in our sample.

2.1. Morphology Classification

We also limit the galaxy sample to spiral galaxies by adopting the morphological classification of the Korea Institute for Advanced Study DR7 Value-Added Galaxy Catalog (KIAS DR7-VAGC; Choi et al. 2010). They adopted an automated classification scheme introduced by Park & Choi (2005) and corrected misclassifications due to the automated scheme by an additional visual inspection.

Then we classify barred galaxies by adopting the barred galaxy catalog provided by Lee et al. (2012). They defined barred galaxies as galaxies with a bar size larger than approximately 25% of the galaxy size by visual inspection. Since the bar fraction is affected by the inclination of galaxies, we also limit the late-type galaxy sample to those with an isophotal axis ratio b/a greater than 0.6.

Our final sample consists of 6195 spiral galaxies with $\sigma > 70$ km s^{-1}, and 1893 (30.6%) are barred and 3754 (60.6%) are non-barred. The rest are weak or ambiguous barred galaxies.

2.2. AGN Selection

Type II AGNs are separated from star-forming galaxies (SFGs) based on the flux ratios of the Balmer and ionization line (BPT diagram; Baldwin et al. 1981). The activity types are classified based on the ratios of emission lines (Hα, Hβ, [O III] λ5007, and [N II] λ6584) that are detected with a signal-to-noise ratio (S/N) of S/N $\geqslant$ 3. We classify the activity types of galaxies using a conservative AGN definition from Kewley et al. (2006) and define an AGN host by combining the composite galaxies and pure AGNs. Some of the weak LINERs are retired galaxies powered by the hot low-mass evolved stars rather than low-luminosity AGNs (Cid Fernandes et al. 2010, 2011). By adopting a criterion of Cid Fernandes et al. (2011), we excluded ambiguous objects with a $W_{\rm H\alpha} < 3$ Å from the pure AGNs. We also excluded potential Type I AGNs that have a Hα emission line width larger than $\sim$500 km s^{-1} (FWHM). Out of 1893 barred spiral galaxies with $\sigma > 70$ km s^{-1}, 805 AGN hosts (42.5%) are found and out of 3754 non-barred ones, 1098 AGN hosts (29.3%) are found.

2.3. Environmental Parameters

Two major environmental factors are considered in this study. One is a large-scale background density ρ_{20} defined by the 20 closest galaxies of a target galaxy in the sample. This density is measured across distances just over a few megaparsecs (see Section 2.5 of Park & Choi 2009 for details). The other environmental factor is the distance between a target galaxy and a pair galaxy, $r_{\rm p}$. Each environment of all the sample galaxies is described by a combination of $r_{\rm p}$ and ρ_{20}. The full details of the estimation of ρ_{20} and $r_{\rm p}$ are described in Park et al. (2008) and Park & Choi (2009).

2.3.1. Large-scale Background Density

The large-scale background density of a target galaxy is given by

$$\rho_{20}(\mathbf{x})/\bar{\rho} = \sum_{i=1}^{20} \gamma_i L_i W_i(|\mathbf{x}_i - \mathbf{x}|)/\bar{\rho}, \quad (1)$$

where the γ_i is the mass-to-light ratio of a background galaxy that is adopted to obtain the mass density described by 20 neighboring galaxies. Here, the ratio of the dark halo virial mass for early- and late-type targets, γ (early) $=2\gamma$ (late), is all that is needed. The $\bar{\rho}$ is a mean density of the universe with a total volume of V, and L_i is the r-band luminosity of the closest 20 background galaxies of a target spiral galaxy. We adopt the spline kernel weighting, W_i, that has an adaptive smoothing scale to include 20 galaxies within the kernel weighting.

2.3.2. The Nearest Neighbor Galaxy

The pair galaxy for a host galaxy is defined using the conditions of the r-band absolute magnitude and radial velocity difference, Δv, as that which is located closest to the target galaxy in the sky. If a host galaxy has M_r, the nearest neighbor galaxy for that host galaxy has $M_r < M_r + 0.5$ and $\Delta v < 400$ km s^{-1}, making it the most influential neighbor. The $\Delta v = 400$ km s^{-1} is obtained by measuring the pairwise velocity difference between target galaxies and their neighbors (see Section 2.4 of Park et al. 2008). The $r_{\rm p}$ measures the impact of interactions with the most influential neighbor (i.e., pair galaxy). The virial radius of the pair galaxy $r_{\rm vir,\ nei}$ is defined as $r_{\rm p}$, where the mean mass density ρ_n within the sphere with a radius of r_p is equal to 740 times the mean density of the universe $\bar{\rho}$. The $r_{\rm vir,nei}$ of spiral galaxies with $M_r = -19.5$ corresponds to 210 h^{-1} kpc.

3. Entangled Effects of Environments and Bars

We begin by showing how the probability of a galaxy hosting an AGN or a bar ($f_{\rm AGN}$ or $f_{\rm bar}$) varies depending on the two central properties of the velocity dispersion, σ, and central star formation rate, SFR$_{\rm fib}$, which are closely related to the BH mass and central star formation (SF), respectively.

Figure 1 shows how $f_{\rm AGN}$ and $f_{\rm bar}$ are related to each other at given SFR$_{\rm fib}$ and σ in the left and middle panels. The right panel is for the bar effect on $f_{\rm AGN}$ defined as a ratio between the $f_{\rm AGN}$ s in the barred and the non-barred galaxies. A ratio greater than 1.0 indicates a positive bar effect on AGN triggering. Colored line contours denote the constant levels of $f_{\rm AGN}$, $f_{\rm bar}$, and bar effect.

All the smoothed distributions that we measure hereafter are obtained using the fixed-size spline kernel for each bin (60 by 60) in the parameter space and contours where a standard error estimated by 1000 bootstrapping sampling is more than 30% of the fraction measurement are eliminated.

The key results are as follows. We have examined the relations using conservatively selected AGNs with an S/N $\geqslant$ 6 in Kim et al. (2020b, see for more details).

1. At a given SFR$_{\rm fib}$ and σ, it is clear that overall, the bar presence has a positive effect on $f_{\rm AGN}$. However, the $f_{\rm bar}$ and the bar effect on $f_{\rm AGN}$ are not directly related. That is, the bar presence itself has little to do with nuclear activity.

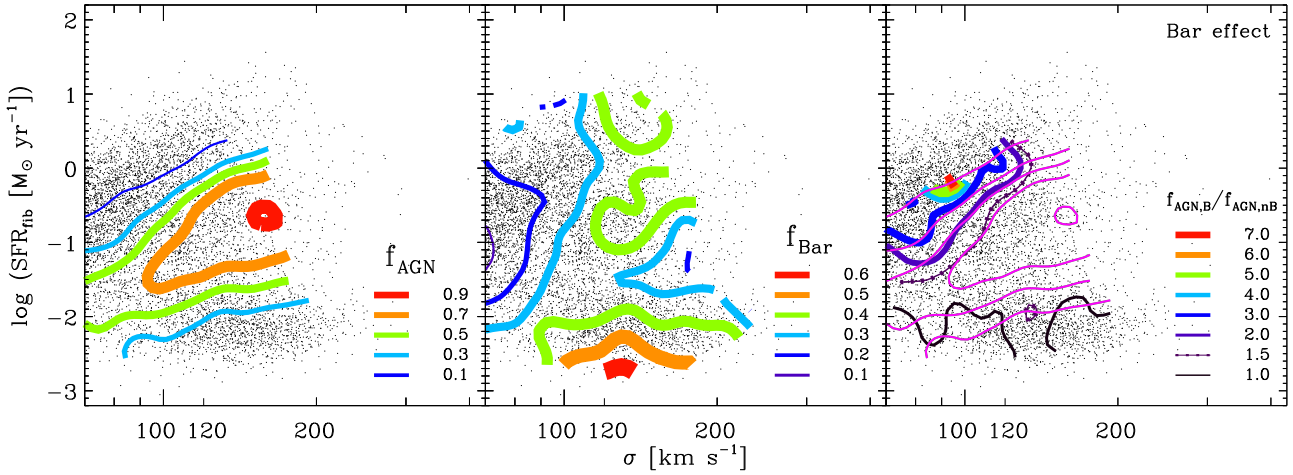

Figure 1. Dependence of AGN fraction (left), bar fraction (middle), and bar effect on $f_{\rm AGN}$ (right) on $\rm SFR_{fib}$ and σ. Points are all galaxies of the sample, and contours show constant levels of each measurement. In the right panel, the contours of $f_{\rm AGN}$ are superimposed in magenta for comparison.

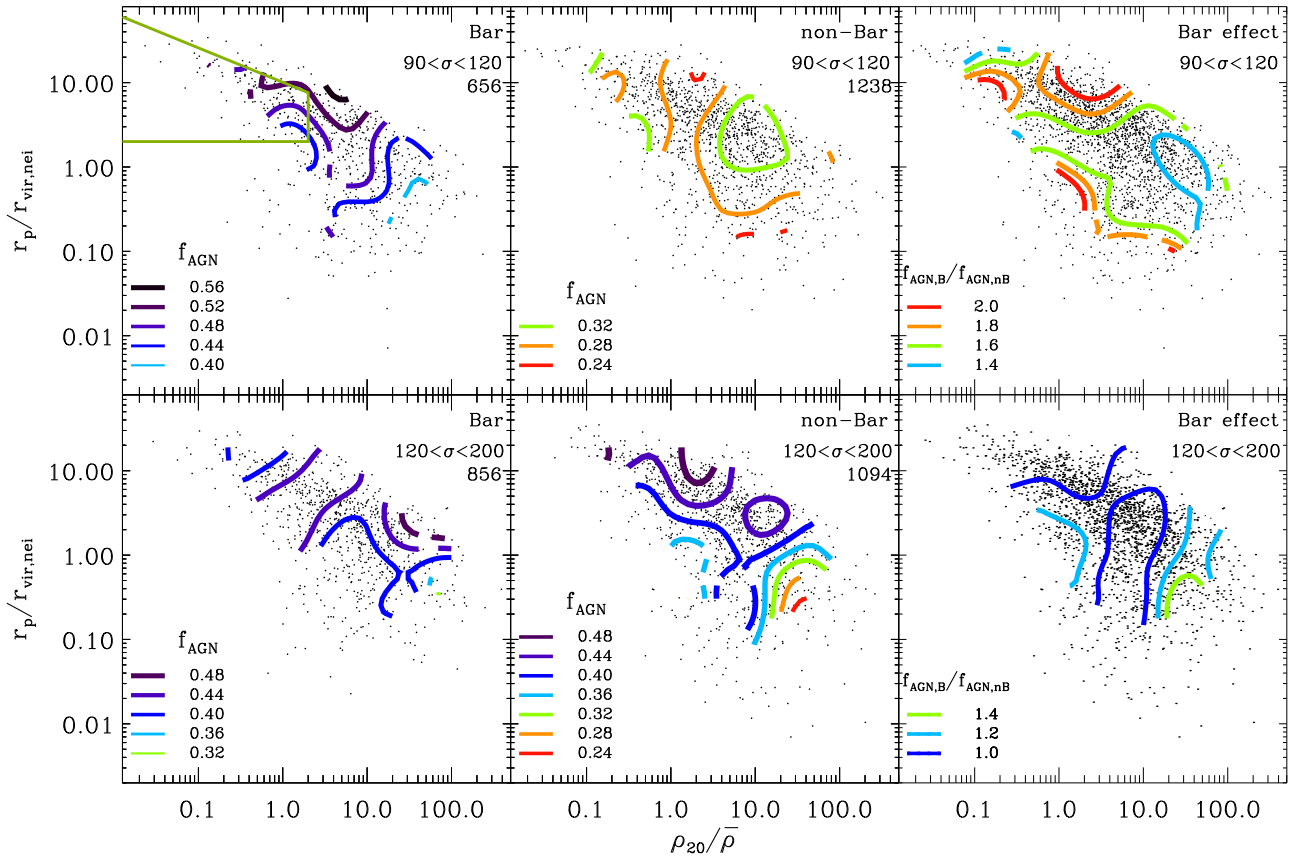

Figure 2. AGN fraction and environment relations. Four cases are given: barred galaxies (left) and non-barred galaxies (middle) with 90 km s^{-1} $< \sigma <$ 120 km s^{-1} (upper) and 120 km s^{-1} $< \sigma <$ 200 km s^{-1} (bottom). An environment of a galaxy is given with the projected pair separation $r_{\rm p}$ and the large-scale background density ρ_{20}. Right panels are for the bar effect on AGN fraction of each subsample. The total galaxy number of each subsample is given in the corresponding panel. The region enclosed by the green lines in the upper left panel represents the isolated environment.

2. In high-σ galaxies having the highest $f_{\rm bar}$ and $f_{\rm AGN}$, the bar effect is the lowest, implying that the BH mass is a key driver of galaxy evolution.
3. The strongest bar effect is found in SFGs leaving the main sequence with high $\rm SFR_{fib}$ and low σ values, although they have low $f_{\rm AGN}$ and $f_{\rm bar}$ values. In galaxies where BH is not massive but actively stars form, bars play an important role in inducing AGNs.

Here a natural question that arises is whether or not the AGN fraction directly depends on environments. To this end, first of all, it is necessary to minimize the effects of the bars and σ. We first divide the sample into two cases with $\sigma >$ 120 km s^{-1} and 90 $< \sigma <$ 120 km s^{-1}. The lower cut of the σ = 90 km s^{-1} is to avoid possible incompleteness. Each sample is further divided into two, according to the presence or absence of a bar. Then we measure $f_{\rm AGN}$ in the $r_{\rm p}$–ρ_{20} space for the four subsamples, as shown in Figure 2.

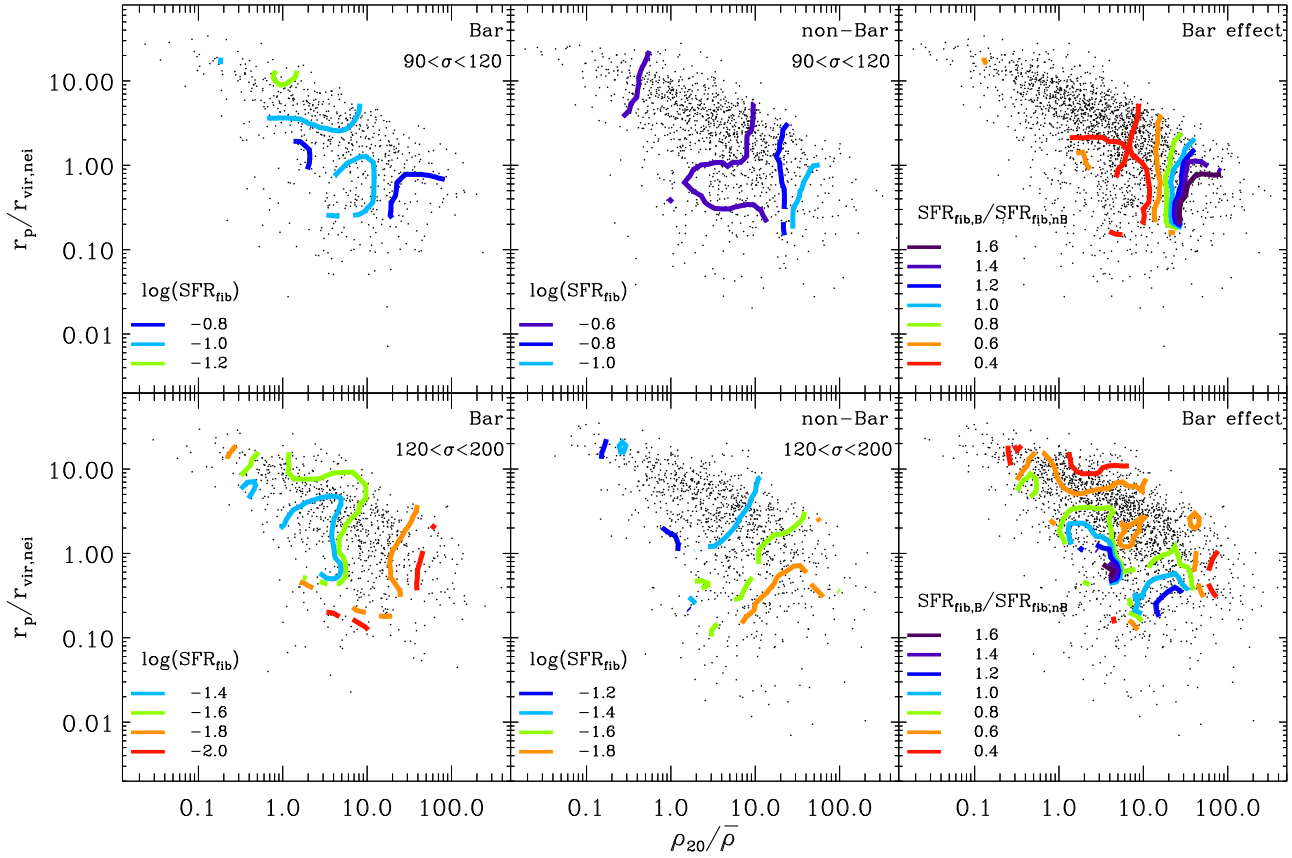

Figure 3. Median contours of SFR_{fib} in the r_p–ρ_{20} space for the four cases (same as in Figure 2). Contours are limited to regions with statistical significance above 1σ. Right panels are for the bar effect on SFR_{fib} of each subsample. A smaller ratio than 1.0 indicates a positive bar effect on SF quenching.

The r_p–ρ_{20} diagram well describes the various environments in which galaxies reside (see Section 3.2.1. of Kim et al. 2020a for details). The ρ_{20} spans various large-scale environments from voids to clusters and the r_p measures the impact of interactions with the most influential neighbor.

For convenience, we define a intermediate-local-density region of $\bar{\rho} < \rho_{20} < 10\bar{\rho}$ and a high-local-density region of $\rho_{20} > 20\bar{\rho}$ as a group environment and cluster environment, respectively.

We also present the changes in SFR_{fib} in the same r_p–ρ_{20} space for the same subsamples, as shown in Figure 3. Note that the median contours of SFR_{fib} are uniformly binned in the logarithm of SFR_{fib}. In the right panels, the bar effects on SFR_{fib} are presented. A smaller ratio than 1.0 indicates a positive bar effect on the central SF "quenching." The values of SFR_{fib} of each σ subsample are somewhat limited due to the σ limit.

Spiral galaxies tend to disappear at smaller r_ps in the cluster environment. Given the morphology–density relation, the inner region of clusters seems to be occupied by elliptical galaxies. A region with a relatively larger $r_p = 1 \sim 2r_{vir,nei}$ corresponds to cluster outskirts. In the group environment, galaxies at $r_p < r_{vir,nei}$ hydrodynamically interact with the closest neighbor, which is enough to change the mean morphology and SF activity of the target galaxies (e.g., Park & Choi 2009).

Meanwhile, we classify galaxies that do not possess a close pair (i.e., large r_p) and are surrounded by few neighbors (i.e., low ρ_{20}) as isolated ones that we use as a control (see Figures 4 and 5). The region enclosed by the green lines in the upper left panel of Figure 2 represents the isolated environment.

Figure 2 shows that AGN triggering depends on the environment, which is different depending on the presence of a bar and the σ value. This finding demonstrates that, when investigating the direct impact of the environment on AGN, it is necessary to limit carefully galactic properties closely related to the central cold gas supply and bulge mass.

In the upper panels, the low-σ subsample clearly shows that overall the barred case has a significantly higher f_{AGN} compared to the non-barred counterpart in a given environment, demonstrating a critical role of bars. This fact is consistent with the third key result of Figure 1.

At the largest r_p in groups, the non-barred case has the highest SFR_{fib} and the lowest f_{AGN}, while the barred case has a relatively lower SFR_{fib} and the highest f_{AGN}. As a result, the bar effect in the largest r_p regions of groups doubles (see the upper right panel). Previous works (Park et al. 2008; Park & Choi 2009) pointed out that the galaxies at the location would be endproducts of mergers and strong interactions.

At the same location in the upper right panel of Figure 3, the ratio between the SFR_{fib} in the barred and the non-barred galaxies is smallest (less than 1.0), indicating that the SF quenching in the galactic center is also strongly accompanied by the bars.

These findings demonstrate that bar instability promotes both central SF quenching and BH feeding in galaxies, seen at the late stage of gas-rich mergers in groups. The anticorrelation between central SFR and AGN activity supports negative feedback (e.g., Silk & Rees 1998; Fabian 2012).

A caveat here is that as Robichaud et al. (2017) pointed out in numerical simulations, AGN-driven outflow in barred hosts

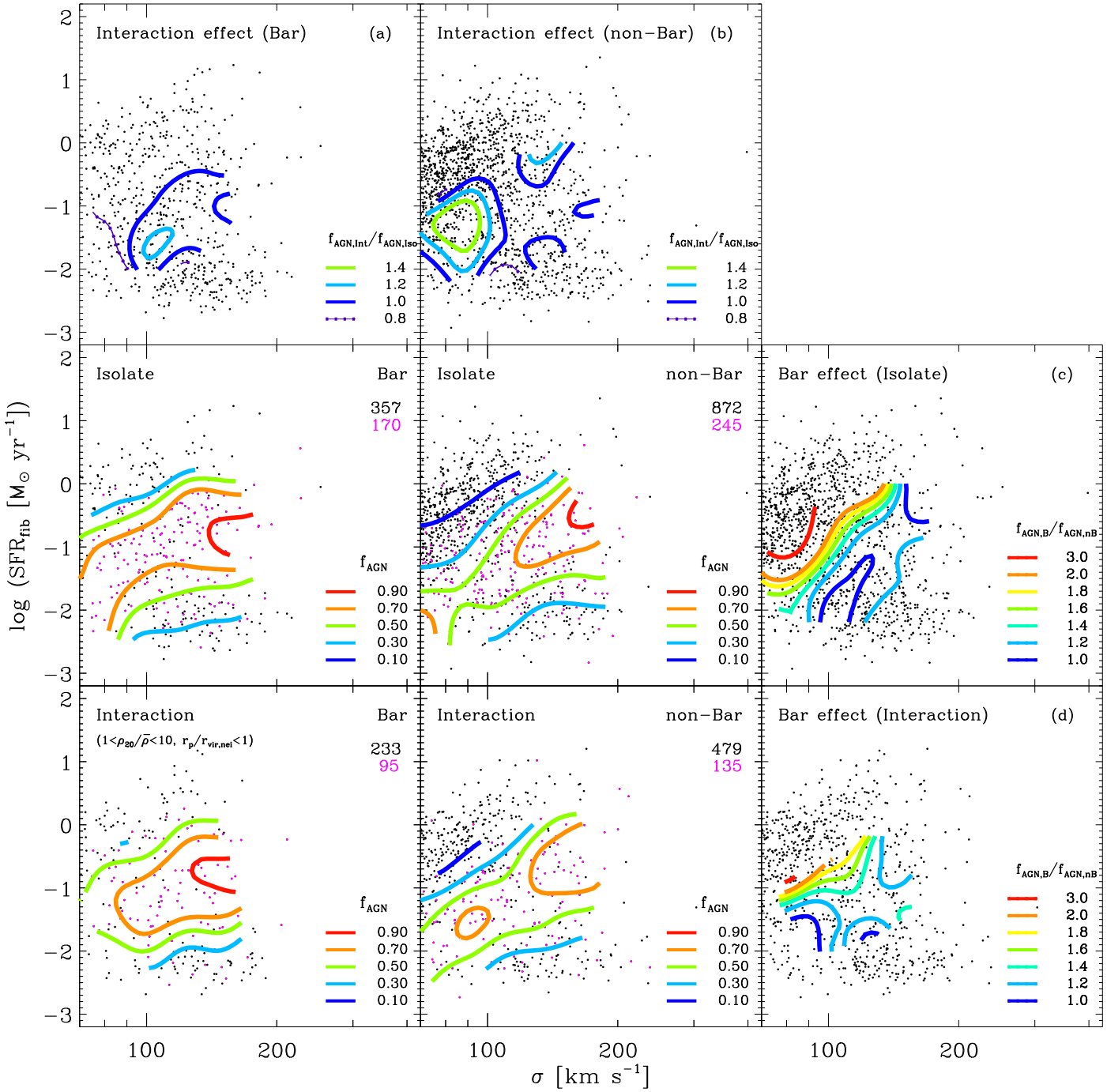

Figure 4. Dependence of f_{AGN} on SFR_{fib}. Four cases are given: barred and non-barred cases located in isolated environments (middle), and barred and non-barred cases interacting with a pair (bottom). The relative effect of a pair interaction is plotted for the barred (panel (a)) and non-barred cases (panel (b)). The isolated cases are used as a control. Panels (c) and (d) are for the bar effect in a given environment. In each subsample, magenta and black points are AGN hosts and non-AGN galaxies, respectively, and their total number is also given in the same color as the points.

can collide with inflowing gas, possibly leading to SF enhancement in the central kiloparsec region (i.e., positive plus negative scenario). Indeed, in Kim et al. (2020b) using the same low-σ sample, we found a tendency that at a given SFR_{fib} and σ, barred cases of AGN hosts have a relatively stronger outflow signature (traced by [O III] velocity dispersion) than non-barred counterparts. In the high-σ sample, the tendency is rare. Assuming that strong outflow of AGNs in barred galaxies causes SF enhancement along with SF quenching, barred AGN hosts could have the same central SFR as that of the non-barred ones.

However, the most pronounced anticorrelation was found in the barred samples of this study, especially in galaxies that have experienced a recent gas-rich merger. Probably due to violent disturbances caused by gas-rich mergers, bars drive larger amounts of gas toward the center, increasing both accretion rate and AGN outflow strength. This feature suggests that the positive feedback effect is not sufficient to mitigate the negative feedback effect, at least within the central region. This

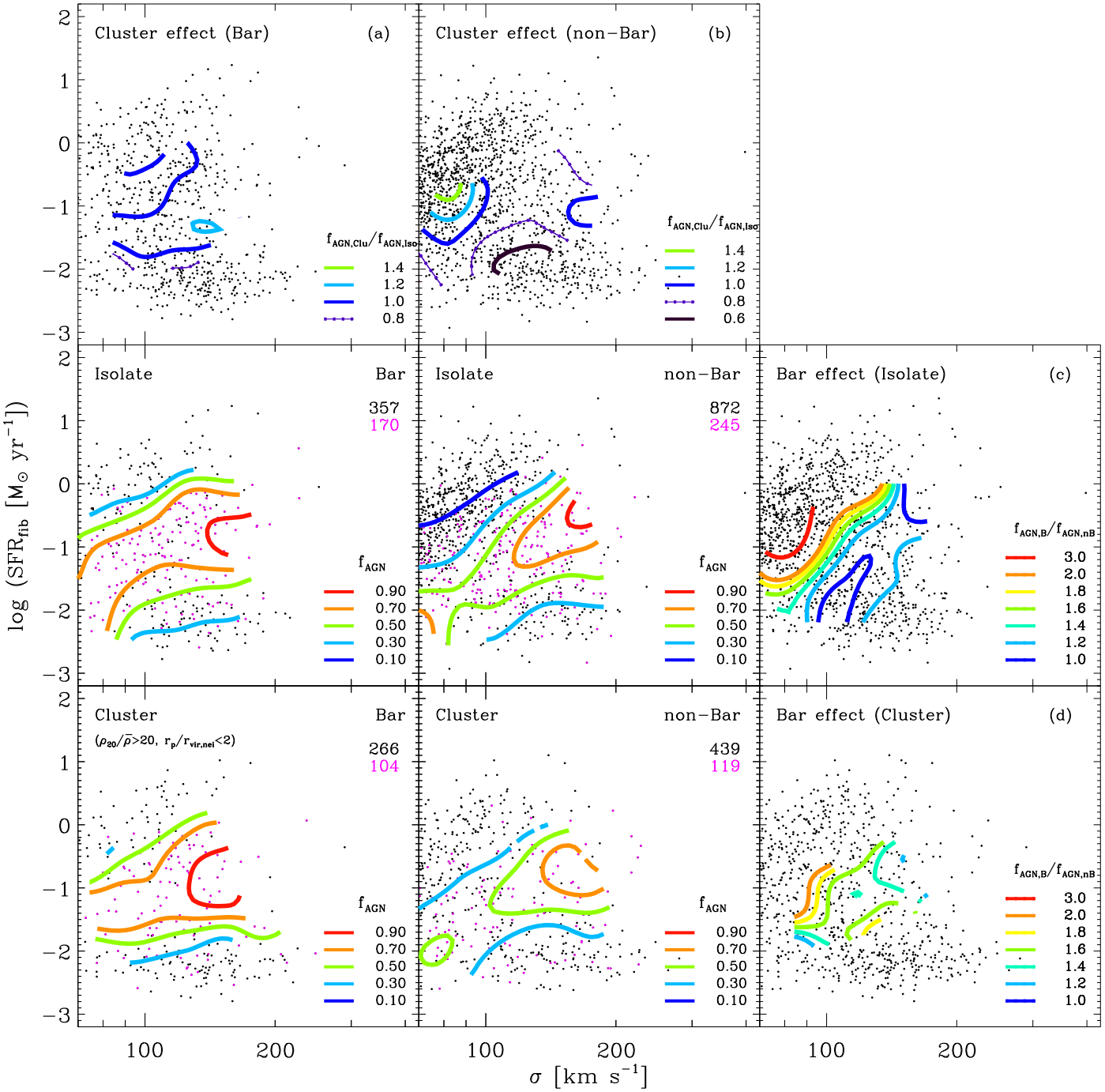

Figure 5. Same as in Figure 4, but for the relative effect of cluster environments.

study shows that barred galaxies with less massive BHs are excellent samples to understand the relation between AGN feedback and galaxy evolution.

Meanwhile, in the lower panels, the high-σ subsample shows a little bar effect overall. The feature is because galaxies with a massive bulge can have high $f_{\rm AGN}$ without bars. The result reveals that the BH mass is a crucial driver of galaxy evolution, consistent with the second key result of Figure 1.

A noticeable bar effect is observed in clusters. Compared to the barred ones, non-barred ones have a sharply decreasing $f_{\rm AGN}$ toward the center. In other words, in galaxies with a massive BH, bar-driven gas inflows are useful only in clusters where there is a deficit of available cold gas fuel. They tend to have a less luminous AGN and red color (see Kim et al. 2020a for details). Alonso et al. (2014) found that the enhancement of nuclear activity is notable in barred active galaxies located in higher-density environments using a massive galaxy sample, consistent with our result.

4. The Relative Importance of a Massive Central Engine, Bars, and Galaxy Interactions

In the previous section, we found in non-barred galaxies that the environmental dependence of $f_{\rm AGN}$ exists even after excluding the effects of bars and bulges. However, their

SFR_{fib} value still has an environmental dependency, which can affect f_{AGN} (in particular, the low-σ case).

Therefore, to properly remove the dependence on the primary central quantities, we measure the f_{AGN} values at given SFR_{fib} and σ. We divide the sample into three different environment cases. Each case is further divided into two cases, those with and without a bar.

The results for a total of six subsamples are shown in Figures 4 and 5. In addition, we measure the relative effects of the pair interaction and cluster environment against the isolated environment for barred and non-barred samples separately. We also measure the bar effect in a given environment. Panel (b) in both figures (i.e., the non-barred case) shows the impact of the environment only, and panel (c) in both figures (i.e., the isolated case) shows the bar effect with a minimal environmental contribution.

Panels (c) and (d) in Figures 4 and 5 demonstrate that bars play the most crucial role when SFGs with lower $\sigma < 100$ km s^{-1} evolve to the starburst–AGN composite hosts, which most favor isolated environments. Conversely, for high-σ galaxies with the largest f_{AGN}, the bar effect is the smallest. For gas-poor galaxies hosting faint AGNs, the bar effect resumes, which is more noticeable in dynamic environments, especially a cluster environment.

In panel (b) of Figures 4 and 5, non-barred galaxies show the σ dependency of the environmental effect. The decisive role of galaxy interactions or cluster environments compared to an isolated environment is only observed at low σ. At high σ, the low value of the bar effect shows how harsh a cluster environment is for AGN triggering.

By comparing panels (a) and (b) in Figures 4 and 5, we infer that once a galaxy has a bar, f_{AGN} enhances overall and is less affected by an environment. The σ dependency of the environmental effect is also not as evident as in non-barred galaxies overall.

By comparing panels (b) and (c) in Figures 4 and 5, we quantify the relative role of a bar and environments. The bar-induced gas inflow is approximately 1.2 to 2 times more efficient at AGN triggering than the external mechanisms. Even the importance of the bar effect tends to be more significant at lower σ. Alonso et al. (2018) suggested that barred AGN hosts show an excess in AGN activity and BH accretion rate compared to AGN hosts with a close pair using a massive galaxy sample, consistent with our result.

We conclude that environmental factors of galaxy interaction or cluster environments play a decisive role in low-σ galaxies. Once there is a large bar in a galaxy, the environmental factors have little impact on AGN triggering. We find the most substantial bar effect when the low-σ galaxies are in isolated environments.

Galaxies with a massive bulge have a high f_{AGN} even without a bar. However, for the red galaxies that have consumed cold gas fuel, the role of the bar becomes critical again, especially when in clusters.

5. Summary

Using an extensive volume-limited sample of spiral galaxies obtained from SDSS DR7, we showed that the AGN fraction of galaxies is quantitatively different depending on the central velocity dispersion and central SF of the host galaxy, bar presence, and galaxy environments.

We found that when galaxies with a massive BH have high central SFRs, AGNs are best triggered, showing that the BH mass is the most crucial driver of spiral galaxy evolution. For galaxies with a less massive BH or galaxies with low central SFRs due to lack of central gas supply, even with a large BH mass, bar instability plays a vital role in galaxy evolution. We found the most substantial effect of bars on AGN in SFGs (i.e., blue galaxies) evolving to AGN host galaxies, consistent with the results of previous studies (Hao et al. 2009; Oh et al. 2012).

We also investigated whether galaxy environments providing other gas inflow mechanisms directly affect AGN activity in the innermost part. Since galaxy environments directly affect the critical ingredients for AGN triggering, such as BH mass, gas fuel, and bar formation, to unveil the direct impact of the galaxy environment, the properties should be carefully limited. Indeed, the role of galaxy environments has often been debated.

The combination of pair interactions and local density well describes the various environments of galaxies, allowing relative comparisons between different environments at a glance. We successfully isolated each effect of bars and galaxy environments.

In particular, this study highlights how directly galaxy environments influence AGN–galaxy coevolution. Gas inflows induced by bars or galaxy environments play a decisive role in BH feeding of galaxies with a less massive BH. In the absence of the massive central engine or gas fuel availability, the role of the additional gas inflow mechanisms becomes critical.

The authors thank Sungsoo S. Kim for helpful comments. This research is supported by the National Research Foundation (NRF) of Korea to the Center for Galaxy Evolution Research (No. 2017R1A5A1070354). M.B.K. is also supported by the BK21 plus program through the NRF funded by the Ministry of Education of Korea.

Funding for the SDSS and SDSS-II has been provided by the Alfred P. Sloan Foundation, the Participating Institutions, the National Science Foundation, the U.S. Department of Energy, the National Aeronautics and Space Administration, the Japanese Monbukagakusho, the Max Planck Society, and the Higher Education Funding Council for England. The SDSS Web site is http://www.sdss.org/.

ORCID iDs

Yun-Young Choi https://orcid.org/0000-0002-3312-1007

References

Abazajian, K. N., Adelman-McCarthy, J. K., Agüeros, M. A., et al. 2009, ApJS, 182, 543
Alonso, M. S., Coldwell, G., Duplancic, F., Mesa, V., & Lambas, D. G. 2018, A&A, 618, 149
Alonso, M. S., Coldwell, G., & Lambas, D. G. 2013, A&A, 549, A141
Alonso, M. S., Coldwell, G., & Lambas, D. G. 2014, A&A, 572, A86
Athanassoula, E. 2003, MNRAS, 341, 1179
Baldwin, J. A., Phillips, M. M., & Terlevich, R. 1981, PASP, 93, 5
Bernardi, M., Sheth, R. K., Annis, J., et al. 2003, AJ, 125, 1817
Blanton, M. R., Eisenstein, D., Hogg, D. W., Schlegel, D. J., & Brinkmann, J. 2005a, AJ, 629, 143
Blanton, M. R., Schlegel, D. J., Strauss, M. A., et al. 2005b, ApJ, 129, 2562
Brinchmann, J., Charlot, S., White, S. D. M., et al. 2004, MNRAS, 351, 1151
Choi, Y.-Y., Han, D.-H., & Kim, S. S. 2010, JKAS, 43, 191
Cid Fernandes, R., Stasińska, G., Mateus, A., & Vale Asari, N. 2011, MNRAS, 413, 1687

Cid Fernandes, R., Stasińska, G., Schlickmann, M. S., et al. 2010, MNRAS, 403, 1036
Ciotti, L., & Ostriker, J. P. 2007, ApJ, 665, 1038
Davies, R., Burtscher, L., Dodds-Eden, K., & Orban de Xivry, G. 2012, JPhCS, 372, 012046
Ellison, S. L., Patton, D. R., Mendel, J. T., & Scudder, J. M. 2011, MNRAS, 418, 2043
Eskridge, P. B., Frogel, J. A., Pogge, R. W., et al. 2000, AJ, 119, 536
Fabian, A. D. 2012, ARA&A, 50, 455
Friedli, D., & Benz, W. 1993, A&A, 268, 65
Galloway, M. A., Willett, K .W., Fortson, L. F., et al. 2015, MNRAS, 448, 3442
Gilmour, R., Gray, M. E., Almaini, O., et al. 2007, MNRAS, 380, 1467
Goulding, A. D., Greene, J. E., Bezanson, R., et al. 2018, PASJ, 70, 37
Hao, L., Jogee, S., Barazza, F. D., Marinova, I., & Shen, J. 2009, in ASP Conf. Ser. 419, Galaxy Evolution: Emerging Insights and Future Challenges, ed. S. Jogee et al. (San Francisco, CA: ASP), 402
Hernquist, L., & Mihos, J. C. 1995, ApJ, 448, 41
Hwang, H. S., Park, C., Elbaz, D., & Choi, Y.-Y. 2012, A&A, 538, A15
Kewley, L. J., Groves, B., Kauffmann, G., & Heckman, T. 2006, MNRAS, 372, 961
Kim, M., Choi, Y.-Y., & Kim, S. S. 2020a, MNRAS, 491, 4045
Kim, M., Choi, Y.-Y., & Kim, S. S. 2020b, MNRAS, 494, 5839
Lee, G.-H., Park, C., Lee, M. G., & Choi, Y.-Y. 2012, ApJ, 745, 125
Li, F., Gu, Y.-Z., Yuan, Q.-R., et al. 2019, MNRAS, 484, 3806
Lynden-Bell, D. 1979, MNRAS, 187, 101
Oh, S., Oh, K., & Yi, S. K. 2012, ApJS, 198, 4
Park, C., & Choi, Y.-Y. 2005, ApJL, 635, L29
Park, C., & Choi, Y.-Y. 2009, ApJ, 691, 1828
Park, C., Gott, J. R., & Choi, Y. Y. 2008, ApJ, 674, 784
Park, C., & Hwang, H. S. 2009, ApJ, 699, 1595
Pimbblet, K. A., & Jensen, P. C. 2012, MNRAS, 426, 1632
Rees, M. J. 1984, ARA&A, 22, 471
Robichaud, F., Williamson, D., Martel, H., et al. 2017, MNRAS, 469, 3722
Roos, N. 1981, A&A, 104, 218
Sabater, J., Best, P. N., & Argudo-Fernández, M. 2013, MNRAS, 430, 638
Sabater, J., Best, P. N., & Heckman, T. M. 2015, MNRAS, 447, 110
Sanders, D. B., Soifer, B. T., Elias, J. H., et al. 1988, ApJ, 325, 74
Silk, J., & Rees, M. J. 1998, A&A, 331, L1
Sivakoff, G. R., Martini, P., Zabludoff, A. I., Kelson, D. D., & Mulchaey, J. S. 2008, ApJ, 682, 803
Springel, V., Di Matteo, T., & Hernquist, L. 2005, ApJL, 620, L79
van den Bergh, S. 2002, AJ, 124, 782
Wada, K., Papadopoulos, P. P., & Spaans, M. 2009, ApJ, 702, 63